Received November 20, 2017, accepted December 31, 2017, date of publication January 11, 2018, date of current version February 28, 2018.

Digital Object Identifier 10.1109/ACCESS.2018.2791978

Stability of FPGA Based Emulator for Half-Bridge Inverters Operated in Stand-Alone and Grid-Connected Modes

TRIET NGUYEN-VAN, (Member, IEEE), RIKIYA ABE, (Member, IEEE), AND KENJI TANAKA, (Member, IEEE)
Internet of Energy Laboratory, Department of Technology Management for Innovation, School of Engineering, The University of Tokyo, Tokyo 113-8656, Japan
Corresponding author: Triet Nguyen-Van (nguyen@tmi.t.u-tokyo.ac.jp)

ABSTRACT In this paper, we present stability of a field programmable gate array (FPGA)-based emulator for single-phase half-bridge inverters operated in stand-alone and grid connected modes. The emulator is not only sufficiently accurate to emulate the characteristic behavior of the inverters, but also is sufficiently simple to be implementable on limited FPGA resources. This implementation enables the inverter developers to evaluate the FPGA-based high-speed controller in the early process by a real-time simulator system, which is unable for offline commercial simulation software packages. The discrete-time models, which are implementable on FPGA, are derived by discretizing the continuous-time models of the inverter using the forward-difference method. The stability analysis for the proposed inverter models showed that the quite small values of internal resistances of the inductors may have a serious effect on the stability, which is one of the most important properties of the inverter mathematical model. The experimental results show that the proposed emulator yields voltage, and current responses, which match with that of the real inverter circuit almost exactly under the same digital controller. The results also show that the responses of the emulators are consistent with the stability analysis for the inverter models.

INDEX TERMS Emulator, FPGA, grid-connected, half-bridge inverters, hysteresis current control, stability, stand-alone.

I. INTRODUCTION

Distributed energy, which is composed of numerous distributed small sources, such as diesel, gas, fuel turbines, and renewable energy, has become a solution to most countries in term of energy security concerns, power quality issues, and emission standards [1]–[3]. A distributed power system can be connected to an existing power grid to supply generated power to the grid, or be operated as a stand-alone isolated system at remote locations [4]–[6]. Inverter technologies play an important role enabling higher efficiency, wider area, and realization of such various distributed power networks [7]–[10]. The conventional method to design an inverter and its controller, which is based on experiments directly, takes a lot of time and cost to develop a new inverter. Nowadays, most inverter designs rely on off-line simulations in the early design stage, and on hardware prototypes in the final design and testing stages [11]–[13].

Due to the requirement of high performance, and the increasing switching frequency to reduce the size of inverters, FPGA-based high-speed digital controllers with sampling frequencies in the MHz level are becoming more and more popular [14]–[16]. However, most commercial off-line simulation software packages are generally slow, and available only for controllers, which are implemented on microprocessor or DSP (Digital Signal Processor) with the sampling frequencies at kHz level. A high-speed FPGA-based, real time emulator can evaluate the high-speed digital controllers, which are also implemented on FPGA, while reducing development time and cost [17]–[20]. Although FPGAs have an advantage in high-speed computation, a complex algorithm usually requires a high-spec FPGA with large resources of programmable logic blocks, which usually is at high-price [21]. To reduce the cost, FPGA-based emulators not only need to be sufficiently accurate to emulate the characteristic behavior of the inverters, but also be sufficiently simple, as to be implementable on limited FPGA logic blocks. This paper presents a FPGA based emulator and its stability analysis for single-phase half-bridge inverters operated in stand-alone and grid connected modes.

The paper is organized as follows. Sections 2, and 3 present the continuous-time models and their stability for the inverter with, and without of considering the internal resistances of the inductors. Their corresponding discrete-time models implementable on FPGA are derived in session 4. The digital hysteresis current control used to assess the emulator is presented in Section 5. In Section 6, the experiment results are shown to illustrate the performances of the proposed emulator. Conclusions are given in Section 7.

II. STABILITY OF CONTINUOUS-TIME MODELS FOR HALF-BRIDGE INVERTER IGNORING INTERNAL RESISTANCES OF INDUCTORS

In this session, we will present continuous-time models and their stabilities for half-bridge inverters operated in stand-alone and grid-connected modes ignoring the internal resistance of the inductors.

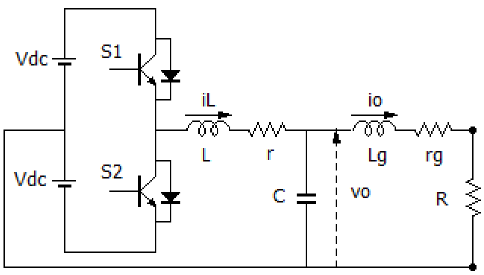

FIGURE 1. Stand-alone inverter circuit.

A. STAND-ALONE MODE INVERTER

Consider a single-phase half-bridge inverter circuit operated in the stand-alone mode shown in Fig. 1 [6], [22]. The DC voltage is supplied by two constant and balanced DC sources, each of which has a value of V_{dc}. Parameters C, L, and L_g present the output capacitor, output inductor, and grid-connected inductor respectively. The internal resistances of the inductors L and L_g are r and r_g, respectively. The output of the inverter is connected to a resistor load R. The inverter is controlled by the switching devices S_1 and S_2.

Let i_L, i_o, and v_o are the ripple current, output current, and output voltage of the inverter, respectively. The values of the internal resistors r and r_g are small, and are ignored in this session ($r = r_g = 0$). Using the Kirchhoff's circuit laws, we can represent the inverter circuit showed in Fig. 1 by a continuous-time model composing of the following three characteristic differential equations

$$\frac{di_L}{dt} = \frac{1}{L}(v_{in} - v_o), \tag{1}$$

$$\frac{dv_o}{dt} = \frac{1}{C}(i_L - i_o), \tag{2}$$

$$\frac{di_o}{dt} = \frac{1}{L_g}(v_o - i_o R), \tag{3}$$

where v_{in} is the control input, which takes the value of $\pm V_{dc}$, corresponding to the ON/OFF state of the switching devices S_1 and S_2.

Let a state vector $\mathbf{x}$ defined by

$$\mathbf{x} = \begin{bmatrix} i_L & v_o & i_o \end{bmatrix}^T. \tag{4}$$

Then, the dynamic linear system given by eqs. (1)-(3) can be written in the vector form as

$$\frac{d\mathbf{x}}{dt} = A\mathbf{x} + bv_{in}, \tag{5}$$

where the system matrix A, and input vector b are given by

$$A = \begin{bmatrix} 0 & -1/L & 0 \\ 1/C & 0 & -1/C \\ 0 & 1/L_g & -R/L_g \end{bmatrix}, \tag{6}$$

$$b = \begin{bmatrix} 1/L & 0 & 0 \end{bmatrix}^T. \tag{7}$$

The characteristic equation [23] of the linear system given by eq. (5) can be written as

$$\lambda^3 + \frac{R}{L_g}\lambda^2 + \frac{1}{C}\left(\frac{1}{L} + \frac{1}{L_g}\right)\lambda + \frac{R}{CLL_g} = 0, \tag{8}$$

where λ is eigenvalue of the system matric A.

The first column of Routh-Hurwitz table [23] for the characteristic polynomial (8) is given by

$$\begin{bmatrix} 1 & R/L_g & R/CL_g^2 \end{bmatrix}^T. \tag{9}$$

The values of R, C, and L_g in eq. (9) are positive. Thus, all these elements of the first column of Routh-Hurwitz table shown by eq. (9) are positive, and the system given by the state equation (5) is asymptotic stable following the Routh–Hurwitz stability criterion [23].

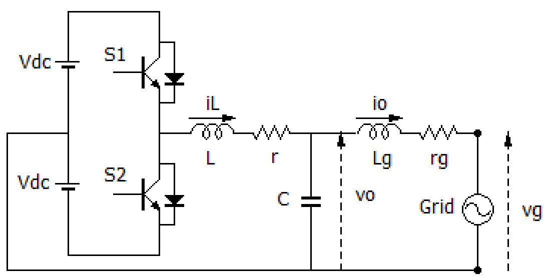

FIGURE 2. Grid-connected inverter circuit.

B. GRID-CONNECTED MODE INVERTER

Consider an inverter, which is similar to that in Section A, but is operated in the grid-connected mode as shown in Figure 2. The output of the inverter is connected to a grid, which has the voltage of v_g.

When the internal resistance r, and r_g are ignored, the characteristic equations for the grid-connected inverter circuit in Fig. 2 are given by

$$\frac{di_L}{dt} = \frac{1}{L}(v_{in} - v_o), \tag{10}$$

$$\frac{dv_o}{dt} = \frac{1}{C}(i_L - i_o), \tag{11}$$

$$\frac{di_o}{dt} = \frac{1}{L_g}\left(v_o - v_g\right). \tag{12}$$

The linear system given by eqs. (10)-(12) can be written in the vector form as

$$\frac{d\mathbf{x}}{dt} = A\mathbf{x} + bv_{in} + cv_g, \tag{13}$$

where the state vector $\mathbf{x}$ is defined as eq. (4). The system matrix A, and vectors b, c are given by

$$A = \begin{bmatrix} 0 & -1/L & 0 \\ 1/C & 0 & -1/C \\ 0 & 1/L_g & 0 \end{bmatrix}, \tag{14}$$

$$b = \begin{bmatrix} 1/L & 0 & 0 \end{bmatrix}^T, \tag{15}$$

$$c = \begin{bmatrix} 0 & 0 & -1/L_g \end{bmatrix}^T. \tag{16}$$

The eigenvalues of the system matrix A can be calculated simply, and are given as

$$\lambda_1 = 0, \lambda_{2,3} = \pm i\sqrt{\frac{1}{C}\left(\frac{1}{L} + \frac{1}{L_g}\right)}. \tag{17}$$

All the eigenvalues of system matrix A have zero real parts. Thus, the linear system given by eq. (13) is not asymptotic stable [24].

III. STABILITY OF CONTINUOUS-TIME MODELS FOR HALF-BRIDGE INVERTER CONSIDERING INTERNAL RESISTANCES OF INDUCTORS

In this session, we consider the same inverter circuit used in Section 2, but with consideration of the internal resistances of the output and grid-connected inductors. Since the values of these internal resistances are quite small, they may change the stabilities of the inverter models, as will be shown as below.

A. STAND-ALONE MODE INVERTER

Using the Kirchhoff's circuit laws, we can present the inverter circuit in Fig. 1 with the non-zero internal resistances ($r, r_g \neq 0$) by the following characteristic differential equations

$$\frac{di_L}{dt} = \frac{1}{L}\left(v_{in} - v_o - ri_L\right), \tag{18}$$

$$\frac{dv_o}{dt} = \frac{1}{C}\left(i_L - i_o\right), \tag{19}$$

$$\frac{di_o}{dt} = \frac{1}{L_g}\left(v_o - \left(R + r_g\right) i_o\right). \tag{20}$$

The vector form of the linear system given by eqs. (18)-(20) can be written as

$$\frac{d\mathbf{x}}{dt} = A\mathbf{x} + bv_{in}, \tag{21}$$

where

$$A = \begin{bmatrix} -r/L & -1/L & 0 \\ 1/C & 0 & -1/C \\ 0 & 1/L_g & -\left(R + r_g\right)/L_g \end{bmatrix}, \tag{22}$$

$$b = \begin{bmatrix} 1/L & 0 & 0 \end{bmatrix}^T. \tag{23}$$

The characteristic equation of system (21) is given by

$$\lambda^3 + \left(\frac{r}{L} + \frac{R + r_g}{L_g}\right)\lambda^2 + \left(\frac{1}{CL} + \frac{1}{CL_g} + \frac{r\left(R + r_g\right)}{LL_g}\right)\lambda + \frac{r + R + r_g}{CLL_g} = 0. \tag{24}$$

The first column of Routh-Hurwitz table for the characteristic polynomial (24) is given by

$$\left[1 \;\; \frac{r}{L} + \frac{R + r_g}{L_g} \;\; \frac{r}{CL^2} + \frac{R + r_g}{CL_g^2} + \frac{r\left(R + r_g\right)}{LL_g} \times \left(\frac{r}{L} + \frac{R + r_g}{L_g}\right)\right]^T. \tag{25}$$

All these elements of the first column of Routh-Hurwitz table (25) are positive. Thus, by using Routh–Hurwitz stability criterion for characteristic eq. (24), we find the system given by (18) is asymptotic stable [23].

B. GRID-CONNECTED MODE INVERTER

The characteristic equations for the circuit in Fig. 2 with the internal resistances r, $r_g \neq 0$ are given by

$$\frac{di_L}{dt} = \frac{1}{L}\left(v_{in} - v_o - i_L r\right), \tag{26}$$

$$\frac{dv_o}{dt} = \frac{1}{C}\left(i_L - i_o\right), \tag{27}$$

$$\frac{di_o}{dt} = \frac{1}{L_g}\left(v_o - v_g - i_o r_g\right). \tag{28}$$

We can write the linear system given by eqs. (26)-(28) in a vector form as

$$\frac{d\mathbf{x}}{dt} = A\mathbf{x} + bv_{in} + cv_g, \tag{29}$$

where

$$A = \begin{bmatrix} -r/L & -1/L & 0 \\ 1/C & 0 & -1/C \\ 0 & 1/L_g & -r_g/L_g \end{bmatrix}, \tag{30}$$

$$b = \begin{bmatrix} 1/L & 0 & 0 \end{bmatrix}^T, \tag{31}$$

$$c = \begin{bmatrix} 0 & 0 & -1/L_g \end{bmatrix}^T. \tag{32}$$

The characteristic equation of system shown in (29) can be written as

$$\lambda^3 + \left(\frac{r}{L} + \frac{r_g}{L_g}\right)\lambda^2 + \left(\frac{1}{CL} + \frac{1}{CL_g} + \frac{rr_g}{LL_g}\right)\lambda + \frac{r + r_g}{CLL_g} = 0. \tag{33}$$

The first column of Routh-Hurwitz table for the characteristic polynomial (33) is given by

$$\left[1 \;\; \frac{r}{L} + \frac{r_g}{L_g} \;\; \frac{1}{C}\left(\frac{r}{L^2} + \frac{r_g}{L_g^2}\right) + \frac{rr_g}{LL_g}\left(\frac{r}{L} + \frac{r_g}{L_g}\right)\right]. \tag{34}$$

All these elements of the first column of Routh-Hurwitz table (34) are positive. Thus, by using Routh–Hurwitz stability criterion for characteristic eq. (33), we find the system given by (29) is asymptotic stable.

The continuous-time models for stand-alone inverter are asymptotic stable either with or without consideration of internal resistances of the inductors. However, for the grid-connected inverter, the model considering internal resistances of the inductors is asymptotic stable, while the model ignoring the internal resistances is not asymptotic stable. Although the values of internal resistances are quite small compared with other electrical components, they may have a serious effect on the stability, which is one of the most important properties of the inverter mathematical model.

IV. DISCRETE-TIME MODELS FOR HALF-BRIDGE INVERTERS

The implementation of the continuous-time models on the FPGA requires their correspondent discrete-time models. Let the clock time interval of the FPGA is T_s. In this session, the discrete-time models for half-bridge inverters are derived by discretizing the proposed continuous-time models in Section 2, and 3 using forward-difference method [25].

Let the continuous-time models of the stand-alone inverter without, and with considering the internal resistances of the inductors are SA_CTM1, and SA_CTM2; the continuous-time models of the grid-connected inverter without, and with considering the internal resistances are GC_CTM1, and GC_CTM2. The models SA_CTM1, SA_CTM2, GC_CTM1, and GC_CTM2 are given by eqs. (1)-(3), (18)-(20), (10)-(12), and (26)-(28) respectively. The correspondent discrete-time versions of these models using forward difference method are SA_DTM1, SA_DTM2, GC_DTM1, and GC_DTM2, given by

1) SA_DTM1

$$i_{L,k+1} = \frac{T_s}{L}\left(v_{in,k} - v_{o,k}\right) + i_{L,k}, \tag{35}$$

$$v_{o,k+1} = \frac{T_s}{C}\left(i_{L,k} - i_{o,k}\right) + v_{o,k}, \tag{36}$$

$$i_{o,k+1} = \frac{T_s}{L_g} v_{o,k} + \left(1 - \frac{T_{ct}R}{L_g}\right) i_{o,k}. \tag{37}$$

2) SA_DTM2

$$i_{L,k+1} = \frac{T_s}{L}\left(v_{in,k} - v_{o,k}\right) + \left(1 - \frac{T_s r}{L}\right) i_{L,k}, \tag{38}$$

$$v_{o,k+1} = \frac{T_s}{C}\left(i_{L,k} - i_{o,k}\right) + v_{o,k}, \tag{39}$$

$$i_{o,k+1} = \frac{T_s}{L_g} v_{o,k} + \left(1 - \frac{T_{ct}\left(R + r_g\right)}{L_g}\right) i_{o,k}. \tag{40}$$

3) GC_DTM1

$$i_{L,k+1} = \frac{T_s}{L}\left(v_{in,k} - v_{o,k}\right) + i_{L,k}, \tag{41}$$

$$v_{o,k+1} = \frac{T_s}{C}\left(i_{L,k} - i_{o,k}\right) + v_{o,k}, \tag{42}$$

$$i_{o,k+1} = \frac{T_s}{L_g} v_{o,k} + \left(1 - \frac{T_{ct}R}{L_g}\right) i_{o,k}. \tag{43}$$

4) GC_DTM2

$$i_{L,k+1} = \frac{T_s}{L}\left(v_{in,k} - v_{o,k}\right) + i_{L,k}, \tag{44}$$

$$v_{o,k+1} = \frac{T_s}{C}\left(i_{L,k} - i_{o,k}\right) + v_{o,k}, \tag{45}$$

$$i_{o,k+1} = \frac{T_s}{L_g} v_{o,k} + \left(1 - \frac{T_{ct}R}{L_g}\right) i_{o,k}, \tag{46}$$

where $i_{L,k}$, $v_{o,k}$, and $i_{o,k}$ are the discrete-time states of the ripple current i_L, the output voltage v_o, and the output current i_o respectively.

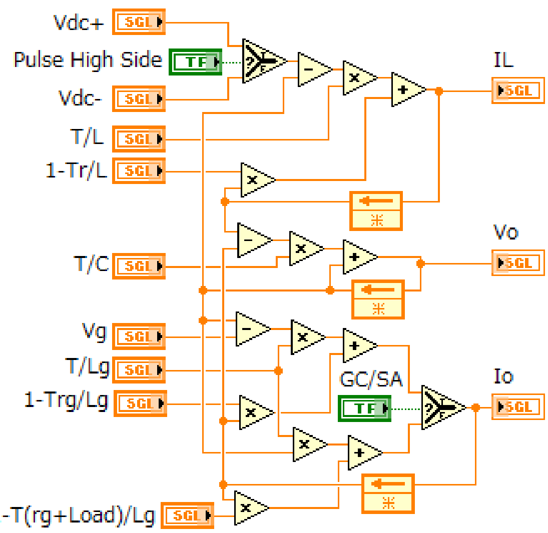

FIGURE 3. LabVIEW program of the discrete-time models for stand-alone and grid-connected inverters.

The above discrete-time models are only composed of addition and multiplication, which are sufficiently simple to be implemented on high speed FPGA. Figure 3 shows the LabVIEW program, which is implemented on FPGA, for the proposed discrete-time models of stand-alone and grid-connected inverters.

V. DIGITAL HYSTERESIS CONTROLLER

There are two main methods to control a switching inverter: linear sine-triangle PWM (Pulse Width Modulation), and hysteresis current control methods. While the popular linear sine-triangle PWM technique requires a PI (Proportional-Integral) regulator to modulate the current error, which may lead to an unavoidable delay [22], [26], the hysteresis current control has fast and stable dynamic response, and does not

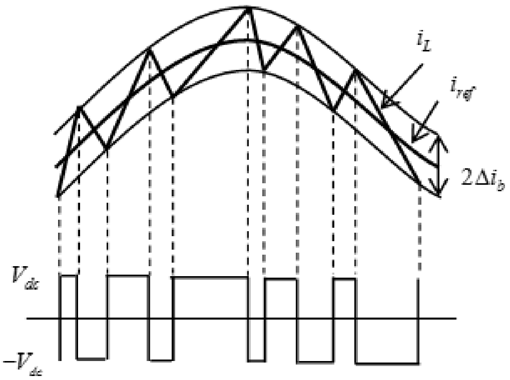

FIGURE 4. Hysteresis current control.

require any information about the system parameters, which enhances its robustness [27], [28]. In this study, the hysteresis current control is applied to control the inverter operated in both stand-alone, and grid-connected modes.

The implementation of hysteresis current control is based on switching signal that is derived by comparison the actual current and the tolerance band around the reference current (Fig. 4). In classical hysteresis controllers, the current band is normally fixed to a certain value, which makes the switching frequency varies to control the current ripple within the band. However, in our study, we use an adaptive hysteresis current control, whose current band is controlled adaptively to maintain the switching frequency at constant. The hysteresis current band is calculated using the measured output voltage and the desired constant switching frequency as [29]

$$\Delta i_{b,k} = \frac{V_{dc}^2 - v_{o,k}^2}{V_{dc}} \frac{T_{sw}}{4L}, \tag{47}$$

where $T_{sw} = 1/f_{sw}$, and f_{sw} is constant switching frequency.

The stand-alone inverter receives the power from DC source to produce a given reference output voltage v_{ref}, which connected to the load. The output voltage is controlled indirectly by the hysteresis current control with the reference current is calculated as [30]

$$i_{ref,k} = i_{o,k} + \frac{v_{ref,k} - v_{o,k}}{T_{sw}} C, \tag{48}$$

where C is the output capacitor of the inverter.

In the grid-connected mode, the output of the inverter is connected to grid directly. The inverter is controlled to supply a given electrical power P to the grid. The reference current used for the hysteresis current control in this case is calculated as

$$i_{ref,k} = \frac{2P}{V_g^2} v_{g,k}, \tag{49}$$

where V_g is the maximum value of the grid voltage.

VI. EXPERIMENTAL RESULTS

The experimental inverter circuit and the control system are shown by Fig. 5. The inverter circuit is designed with the

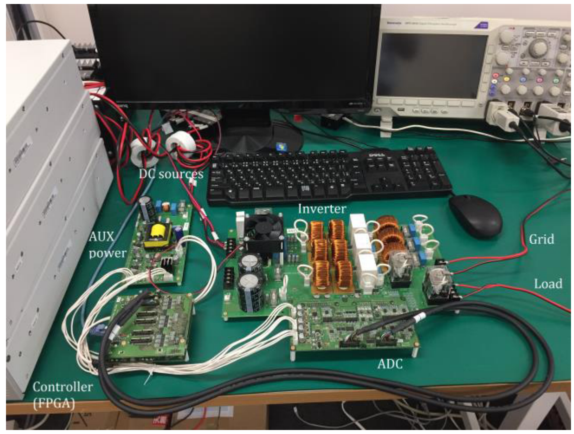

FIGURE 5. Experiment inverter system.

electrical components given by $L = 2.2$ 4mH, $C = 6.8$ μF, and $L_g = 1.1$ mH. The internal resistances of the inductors are $r = 0.3$ Ω and $r_g = 0.15$ Ω respectively.

The voltage and current of the inverter circuit are measured by the analog sensors and sent to the FPGA based controller through an analog/digital converter (ADC), which has the sampling frequency of 4 MHz. The emulator is implemented on the same FPGA with the clock frequency at 120 MHz. The switching frequency used for hysteresis current control is at 20 kHz. The DC voltages of the inverter are supplied by DC generators, and set at $V_{dc} = 175$ V.

A. STAND-ALONE MODE INVERTER

The output voltage of the inverter in stand-alone mode was controlled to produce a reference ac voltage, which is given by

$$v_{ref} = 100\sqrt{2} \sin(100\pi t) \text{ V}. \tag{50}$$

The output of the inverter was connected to a load, which had a value of $R = 100$ Ω.

Figures 6-8 show the voltage and current responses of the real inverter circuit, the emulators with and without consideration of the internal resistances respectively, using the same controller. Both these emulators yield voltage and current responses (Fig. 7, 8), which are stable, and match almost exactly with that of the inverter circuit (Fig. 6). There is no difference between the emulators with and without considering the internal resistances of the inductors. Figures 9, 10 show the responses of the real inverter circuit, and the emulator with considering internal resistances when the load is injected into the output of the inverter. The voltage and current responses of the emulator are very close to that of the real inverter circuit. The emulator also gives good performance with the reference DC voltage.

B. GRID-CONNECTED MODE INVERTER

The output of the inverter was connected to a grid, which had the ac voltage of 100 V, 50 Hz. The inverter was controlled to send a power of $P = 100$ W to the grid.

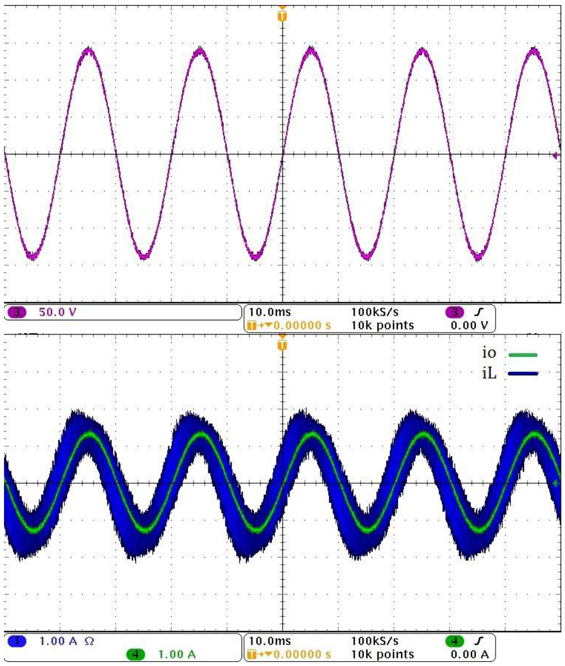

FIGURE 6. Voltage and current responses of the inverter circuit in stand-alone mode.

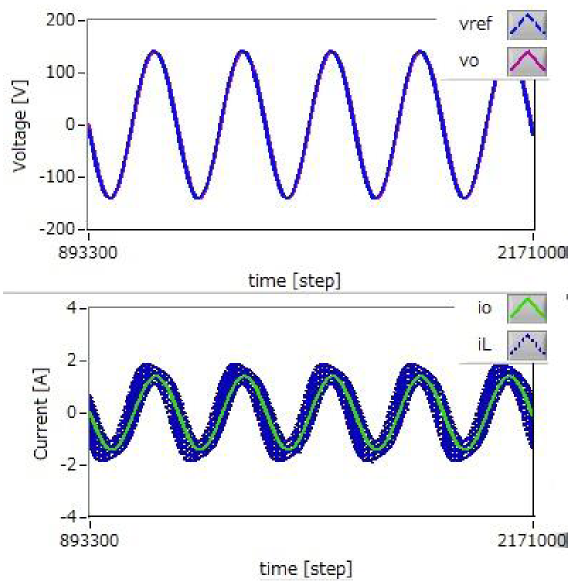

FIGURE 7. Voltage and current responses of the emulator in stand-alone mode ignoring the internal resistances.

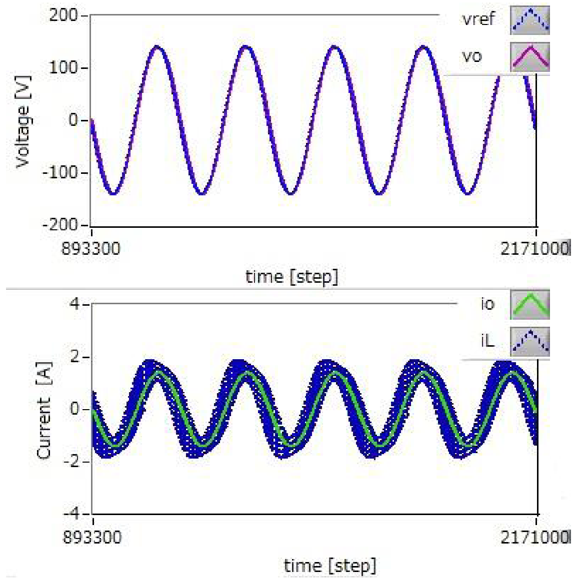

FIGURE 8. Voltage and current responses of the emulator in stand-alone mode considering the internal resistances.

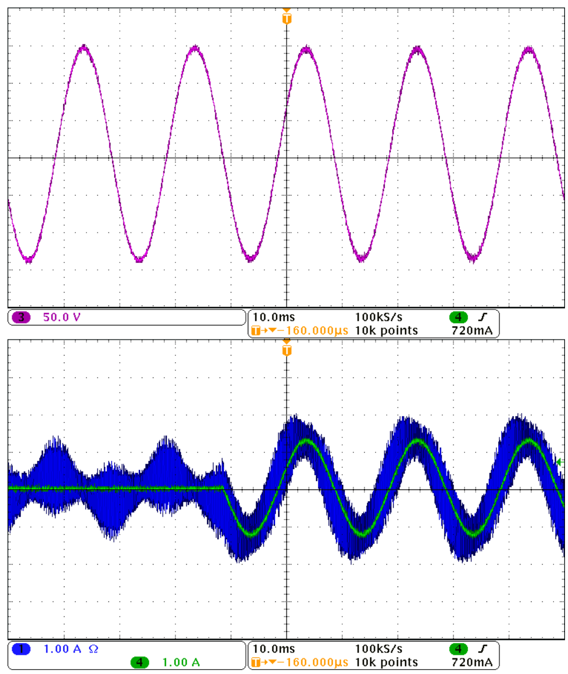

FIGURE 9. Voltage and current responses of the inverter circuit in stand-alone mode with load injection.

Figures 11-13 show the voltage and current responses of the real inverter circuit, the emulators with and without consideration of the internal resistances respectively, using the same controller. The emulator considering the internal resistances yields the voltage and current responses (Fig. 12), which are stable, and match almost exactly with that of the inverter circuit (Fig. 11). While, the voltage and current responses of the emulator ignoring the internal resistances oscillate, and differ from that of the real inverter circuit (Fig. 13). These experimental results are consistent with the stability analysis in session 3.

VII. CONCLUSION

A FPGA based emulator with stability analysis has been proposed for single-phase half-bridge inverters operated in stand-alone and grid connected modes. The emulator is not only sufficiently accurate to emulate the characteristic behavior of the inverters, but is also sufficiently simple to be

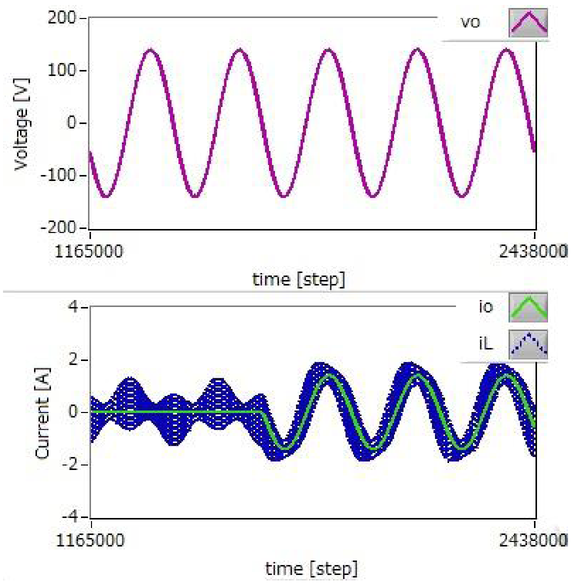

FIGURE 10. Voltage and current responses of the emulator in stand-alone mode with load is injection.

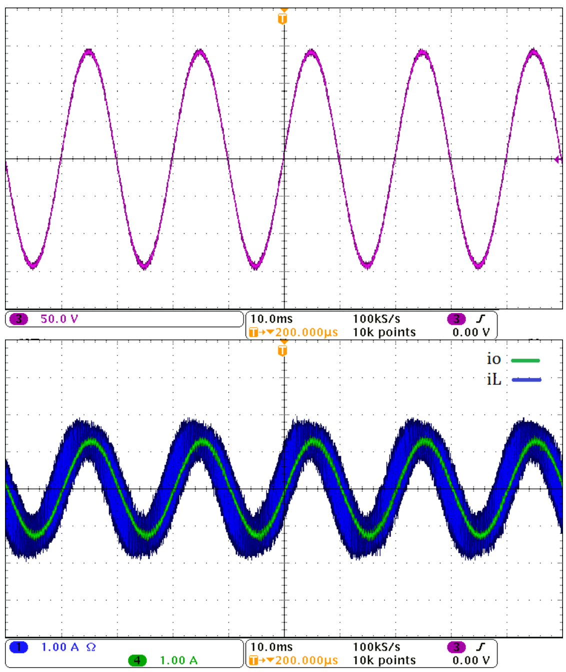

FIGURE 11. Voltage and current responses of the inverter circuit in grid-connected mode.

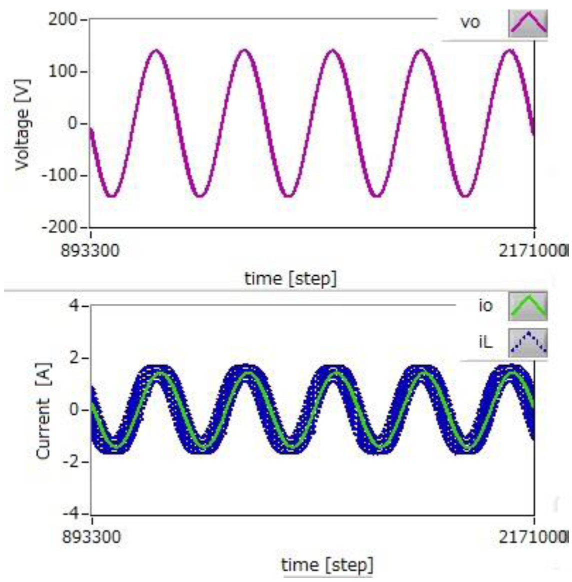

FIGURE 12. Voltage and current responses of the emulator in grid-connected mode considering the internal resistances.

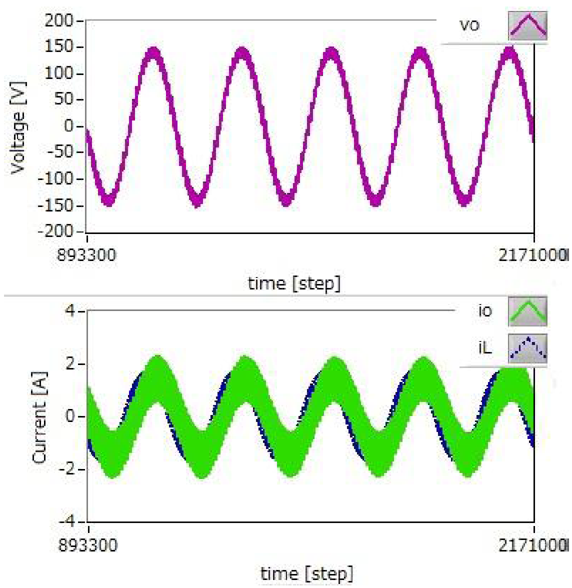

FIGURE 13. Voltage and current responses of the emulator in grid-connected mode ignoring the internal resistances.

implementable on limited FPGA resources. This implementation enables inverter developer to evaluate the FPGA based high-speed controller as a real-time simulator system, which is unable for offline commercial simulation software. The stability analysis for the proposed inverter models showed that both of the models for the stand-alone inverter with and without consideration of the internal resistances of the inductors are stable. However, for the grid-connected inverter, the model considering the internal resistances is stable, while the one ignoring the internal resistances is not. The emulators were assessed by using the FPGA-based digital adaptive hysteresis control with the sampling frequency at 4 MHz. The experimental results show that the proposed emulator yields voltage, and current responses, which match with that of the real inverter circuit almost exactly under the same digital controller. The results also show that the responses of the emulators are consistent with the stability analysis for the inverter models.

REFERENCES

[1] A. Asrari, T. Wu, and S. Lotfifard, "The impacts of distributed energy sources on distribution network reconfiguration," *IEEE Trans. Energy Convers.*, vol. 31, no. 2, pp. 606–613, Jun. 2016.

[2] J. Driesen and F. Katiraei, "Design for distributed energy resources," *IEEE Power Energy Mag.*, vol. 6, no. 3, pp. 30–40, May 2008.

[3] X. Yu, C. Cecati, T. Dillon, and M. G. Simões, "The new frontier of smart grids," *IEEE Ind. Electron. Mag.*, vol. 5, no. 3, pp. 49–63, Sep. 2011.

[4] M. G. Simoes and F. A. Farret, *Modeling Power Electronics and Interfacing Energy Conversion Systems*. Hoboken, NJ, USA: Wiley, 2016.

[5] D. P. Kaundinya, P. Balachandra, and N. H. Ravindranath, "Grid-connected versus stand-alone energy systems for decentralized power—A review of literature," *Renew. Sustain. Energy Rev.*, vol. 13, no. 8, pp. 2041–2050, 2009.

[6] R.-J. Wai, C.-Y. Lin, Y.-C. Huang, and Y.-R. Chang, "Design of high-performance stand-alone and grid-connected inverter for distributed generation applications," *IEEE Trans. Ind. Electron.*, vol. 60, no. 4, pp. 1542–1555, Apr. 2013.

[7] V. G. Agelidis, G. D. Demetriades, and N. Flourentzou, "Recent advances in high-voltage direct-current power transmission systems," in *Proc. IEEE Int. Conf. Ind. Technol.*, Dec. 2006, pp. 206–213.

[8] H. Farhangi, "The path of the smart grid," *IEEE Power Energy Mag.*, vol. 8, no. 1, pp. 18–28, Jan./Feb. 2010.

[9] R. Abe, H. Taoka, and D. McQuilkin, "Digital grid: Communicative electrical grids of the future," *IEEE Trans. Smart Grid*, vol. 2, no. 2, pp. 399–410, Jun. 2011.

[10] J. J. Justo, F. Mwasilu, J. Lee, and J.-W. Jung, "AC-microgrids versus DC-microgrids with distributed energy resources: A review," *Renew. Sustain. Energy Rev.*, vol. 24, pp. 387–405, Aug. 2013.

[11] H. Alatrash, A. Mensah, E. Mark, G. Haddad, and J. Enslin, "Generator emulation controls for photovoltaic inverters," *IEEE Trans. Smart Grid*, vol. 3, no. 2, pp. 996–1011, Jun. 2012.

[12] L. Sinopoli, M. Ordonez, and J. Quaicoe, "DSP-based marine current turbine emulator using a 3-phase inverter," in *Proc. IEEE Energy Convers. Congr. Expo. (ECCE)*, Sep. 2012, pp. 2805–2810.

[13] H. Akbarian, P. Pillay, and L. Lopes, "Design of a power electronic emulator for parallel operation of renewable energy resources in micro-grids," in *Proc. IEEE Int. Electr. Mach. Drives Conf. (IEMDC)*, May 2015, pp. 1532–1537.

[14] A. Belkheiri, S. Aoughellanet, M. Belkheiri, and A. Rabhi, "FPGA based control of a PWM inverter by the third harmonic injection technique for maximizing DC bus utilization," in *Proc. 3rd Int. Conf. Control, Eng. Inf. Technol. (CEIT)*, May 2015, pp. 1–7.

[15] J. O. Krah, M. Holtgen, A. Rath, and R. Richter, "FPGA-based control of three-level inverters," in *Proc. Int. Exhib. Conf. Power Electron., Intell. Motion Power Quality*, 2011, pp. 394–400.

[16] R. Ekström and M. Leijon, "FPGA control implementation of a grid-connected current-controlled voltage-source inverter," *J. Control Sci. Eng.*, vol. 2013, Jan. 2013, Art. no. 14.

[17] J. Chavarria, D. Biel, F. Guinjoan, A. Poveda, F. Masana, and E. Alarcon, "FPGA-based design of a step-up photovoltaic array emulator for the test of PV grid-connected inverters," in *Proc. IEEE 23rd Int. Symp. Ind. Electron. (ISIE)*, Jun. 2014, pp. 485–490.

[18] T. Nguyen-Van, E. Maeda, and R. Abe, "FPGA based emulator for half-bridge inverters operated in stand-alone mode," in *Proc. IEEE Int. Conf. Consum. Electron.-Taiwan (ICCE-TW)*, Jun. 2017, pp. 197–198.

[19] M. A. Kinsy *et al.*, "High-speed real-time digital emulation for hardware-in-the-loop testing of power electronics: A new paradigm in the field of electronic design automation (EDA) for power lectronics systems," in *Proc. Int. Exhib. Conf. Power Electron., Intell. Motion Power Quality*, 2011, pp. 485–490.

[20] J. Poon, E. Chai, I. Čelanović, A. Genić, and E. Adzic, "High-fidelity real-time hardware-in-the-loop emulation of PMSM inverter drives," in *Proc. Energy Convers. Congr. Expo. (ECCE)*, Sep. 2013, pp. 1754–1758.

[21] S. Che, J. Li, J. W. Sheaffer, K. Skadron, and J. Lach, "Accelerating compute-intensive applications with GPUs and FPGAs," in *Proc. Symp. Appl. Specific Process.*, Jun. 2008, pp. 101–107.

[22] S. Ang and A. Oliva, *Power-Switching Converters* (Electrical and Computer Engineering), 2nd ed. Boca Raton, FL, USA: Taylor & Francis, 2005.

[23] R. C. Dorf and R. H. Bishop, *Modern Control Systems*, 11th ed. Upper Saddle River, NJ, USA: Prentice-Hall, 2008

[24] N. S. Nise, *Control System Engineering*, 3rd ed. New York, NY, USA: Wiley, 2000.

[25] T. Nguyen-Van and N. Hori, "New class of discrete-time models for non-linear systems through discretisation of integration gains," *Control Theory Appl., IET*, vol. 7, no. 1, pp. 80–89, Jan. 2013.

[26] M. H. Rashid, *Power Electronics Handbook* (Academic Press Series in Engineering). San Diego, CA, USA: Academic, 2001.

[27] S. Buso, L. Malesani, and P. Mattavelli, "Comparison of current control techniques for active filter applications," *IEEE Trans. Ind. Electron.*, vol. 45, no. 5, pp. 722–729, Oct. 1998.

[28] M. P. Kazmierkowski, R. Krishnan, F. Blaabjerg, *Control in Power Electronics Selected Problems*. San Diego, CA, USA: Academic, 2002

[29] S. Poulsen and M. A. E. Andersen, "Hysteresis controller with constant switching frequency," *IEEE Trans. Consum. Electron.*, vol. 51, no. 2, pp. 688–693, May 2005.

[30] T. Nguyen-Van and R. Abe, "An indirect hysteresis voltage digital control for half bridge inverters," in *Proc. IEEE 5th Global Conf. Consum. Electron.*, Oct. 2016, pp. 612–615.

TRIET NGUYEN-VAN (M'14) received the B.S., M.S., and Ph.D. degrees in system control engineering from the University of Tsukuba, Japan, in 2010, 2012, and 2015, respectively. He is currently a Project Assistant Professor with The University of Tokyo. His research interests include sampled-data control, nonlinear control, power control, and smart-grid.

Dr. Nguyen-Van is member of the ASME and SICE.

RIKIYA ABE (M'08) received the degree in electronics engineering from The University of Tokyo, Japan, and the Ph.D. degree from Kyushu University, Japan. He was with Electric Power Development Company, Tokyo, the Electric Power Research Institute, USA, and The University of Tokyo. Since 2008, he has been a Professor with The University of Tokyo, where he is teaching undergraduate students at the Program for Social Innovation and graduate students at Technology Management for Innovation. His special fields of interests include renewable energy, energy storage, and smart grid.

KENJI TANAKA received the B.E. degree in naval architecture, the M.E. degree in information engineering, and the Ph.D. degree in systems innovation from The University of Tokyo, Tokyo, Japan, in 1998, 2000, and 2009, respectively. He is currently a Project Associate Professor with the Department of Systems Innovations, Graduate School of Engineering, The University of Tokyo. Since 2011, he has been the Director of the Digital Grid Consortium. His current research interests include digital-grid, energy storage systems, battery life-evaluation, electric vehicles, data mining, and demand forecasting.